Earthquakes and Structures, *Vol. 30, No. 5 (2026) 591-609*
https://doi.org/10.12989/eas.2026.30.5.591

Techno-Press

Evaluation criteria for seismic performance and carbon emission assessment methodology of wire-mesh concrete sandwich walls

Hao Wang[1,2a], Wenqi Lu[4], Wenyu Tian[4], Wentao Qiao*[3], Chao Luo[3b]

[1]*Institute of Engineering Mechanics, China Earthquake Administration, Harbin 150080, China*
[2]*Key Laboratory of Earthquake Engineering and Engineering Vibration, Institute of Engineering Mechanics, China Earthquake Administration, Harbin 150080, China*
[3]*Key Laboratory of Road and Railway Engineering Safety Control (Ministry of Education), Shijiazhuang Tiedao University, Shijiazhuang 050043, China*
[4]*School of Civil Engineering, Shijiazhuang Tiedao University, Shijiazhuang 050043, China*

(Received January 18, 2026, Revised February 26, 2026, Accepted March 25, 2026)

Abstract. Wire-mesh concrete sandwich walls (WCWs) represent a composite structural system known for its lightweight construction and low-carbon advantages. However, standardized criteria for evaluating their seismic performance remain insufficient, and quantitative assessments of their carbon reduction potential lack rigorous scientific validation—factors that hinder broader engineering application. In this study, incremental dynamic analysis (IDA) and quantile regression were employed to establish, for the first time, a three-tier seismic performance evaluation framework for WCWs based on inter-story drift ratio and inter-story shear force. Furthermore, a novel four-stage correlation model linking seismic intensity measures (IM), structural response, wall dimensions, and carbon emissions was developed to quantitatively relate seismic design parameters to embodied carbon emissions. This model provides a theoretical basis for the integrated design of structural safety and sustainability in green buildings. A case study of a WCW building demonstrated a 41.19% reduction in carbon emissions compared to conventional reinforced concrete shear walls. These findings offer critical theoretical and technical insights for the application of WCWs in sustainable construction.

Keywords: carbon emission model; incremental dynamic analysis; seismic performance evaluation; wire-mesh concrete sandwich wall

1. Introduction

The accelerating pace of global climate change and rapid urbanization has elevated energy efficiency, carbon emission reduction, and seismic safety to critical priorities in the construction sector. Conventional reinforced concrete (RC) structures, while widely used in civil engineering, have increasingly prominent limitations over time, including high carbon emissions, inconvenient construction, and poor adaptability to modularization. In this context, an innovative composite

*Corresponding author, Professor, E-mail: tottyer@126.com
[a] Ph.D., E-mail: wanghao@stdu.edu.cn
[b] Ph.D., E-mail: luochao@stdu.edu.cn

http://www.techno-press.org/eas/5
ISSN: 2092-7614 (Print), 2092-7622 (Online)

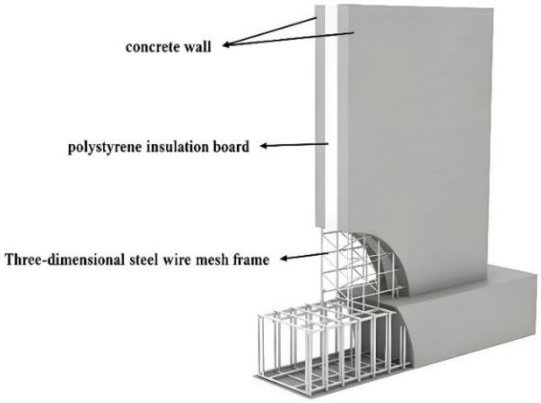

Figure 1. Configuration and structural details of WCW

wall system—the wire-mesh concrete sandwich wall (WCW)—has been developed. As illustrated in Fig. 1, WCWs comprise orthogonally welded wire meshes, diagonal shear connectors, concrete wythes, and an expanded polystyrene (EPS) insulation core. The diagonal connectors are resistance-spot-welded to the wire meshes on both faces, providing composite action between the concrete wythes and core material. This configuration delivers significant advantages in lightweight construction, enhanced thermal performance, low-carbon characteristics, and constructability efficiency (modular assembly). These attributes establish WCWs as a promising solution for sustainable seismic-resistant structures, motivating this research. Despite demonstrating favorable mechanical properties and environmental benefits, the absence of standardized seismic performance evaluation criteria and scientifically validated methodologies for quantifying carbon reduction advantages impedes their broader engineering implementation.

In view of the above problems, scholars have carried out some research on the seismic performance evaluation method of sandwich walls. Hu et al. [1] implemented high-damping viscoelastic isolation mitigation devices (VEIMDs) in precast sandwich wall systems to enhance seismic performance through fundamental period elongation and damping enhancement. He et al. [2] introduced multi-directional viscoelastic dampers (MDVDs) for bolted precast concrete sandwich wall panel structures (PC-SWPS), conducting fragility analyses demonstrating 30-40% reductions in peak floor acceleration (PFA) and interstory drift ratio (IDR). Yan et al. [3] a new type of UPSSW is proposed. Its seismic performance is verified by experiments and simulations, and the optimization design method and bearing capacity calculation formula are established. Li et al. [4] proposes a prefabricated ceramsite foam concrete sandwich shear wall (CFCW) integrating thermal insulation and structural strength, with experimental and numerical analyses revealing the effect of axial compressive ratios on seismic performance. Romina et al. [5] experimentally validated that cavity brick walls retrofitted with glass fiber-reinforced polymer (GFRP) bars and fabric-reinforced cementitious matrix (FRCM) systems exhibited higher in-plane shear capacity and greater out-of-plane resistance. Chougule et al. [6] compared the response differences between prefabricated and monolithic structures under various earthquakes. Gang et al. [7] showed that the seismic performance of the prefabricated sandwich wall (SW) structure is slightly better than that of the cast-in-place form, but it is equivalent to the collapse resistance of the conventional shear wall (RW), and saves material optimization construction. Xiuhua et al. [8] discussed the influence of steel plate configuration parameters (layout, thickness, single and double sides) on the seismic

performance of cold-formed thin-walled steel-paper straw board-steel plate composite wall, and established the calculation formula of shear capacity of composite wall. Fei et al. [9] proposed a precast concrete-filled steel tube boundary single-layer reinforced shear wall structure, which can form an assembled seismic system by connecting the frame beam with bolts. The influence of axial compression ratio and steel bar support on the seismic performance of the structure was analyzed, and a normal section calculation model for predicting the bearing capacity of the structure was proposed. Herrera et al. [10] verified that the two kinds of precast iron wall (PFW) were in the direct occupancy (IO) performance level under earthquake by cyclic loading test combined with Mostaghel hysteresis model and incremental dynamic analysis (IDA), which confirmed its excellent energy dissipation capacity and damage control characteristics. Guo et al. [11] proposed a new type of low-level pre-bolted connection. While these studies have significantly advanced the understanding of sandwich wall seismic behavior—focusing on parameters such as lateral strength, failure modes, and the influence of connectors—a standardized framework that quantitatively links fundamental performance indicators (strength, stiffness degradation, ductility, and energy dissipation) to distinct seismic performance levels (e.g., Immediate Occupancy, Life Safety) remains underdeveloped. This gap hinders the application of performance-based seismic design (PBSD) principles to WCW structures.

At the same time, scholars have also done a lot of research on carbon emission assessment methods for sandwich walls, shear walls and fabricated structures. Tanmay et al. [12] used Life Cycle Assessment (LCA) and Life Cycle Cost Analysis (LCCA) to show that buildings employing precast sandwich wall panels reduce costs and environmental impacts compared to cast-in-situ systems. Xu et al. [13] challenges the assumption that prefabrication ensures decarbonization, revealing its carbon mitigation potential is critically dependent on structural material choices and prefabrication rates, with concrete variants risking carbon lock-in. Dong et al. [14] Prefabrication does not guarantee lower carbon emissions, with an optimal prefabrication rate of 3.8-10.6% needed to balance cost and carbon reduction. Norma et al. [15] compared the sustainability of two semi-sandwich partition panels (APXPS-alkali-activated ceramic/slag waste cement with XPS foam; APICB-alkali-activated ceramic/slag waste cement with expanded cork board) against traditional heavy partitions, lightweight gypsum boards, and conceptual sandwich membrane structures using LCA and multi-criteria decision analysis, finding APXPS and APICB offered optimal environmental-functional-economic performance with negative contributions to global warming potential. Yu et al. [16] explored the potential of advanced engineered wood, enhanced through multi-scale computational design, chemical modification, and structural engineering for improved mechanical, thermal, optical, and energy properties, as carbon-storing materials for sustainable negative-carbon buildings, combining LCA and techno-economic analysis. Hao et al. [17] developed a BIM-based method for quantifying embodied carbon emissions, confirming BIM's effectiveness and revealing the carbon reduction advantages of prefabrication over traditional construction. A.O. et al. [18] studied bio-inspired lightweight sandwich CFRP composites and recycled concrete as steel alternatives, highlighting significant cost-effectiveness, ductile failure modes, and transportation weight reduction benefits, while utilizing recycled aggregates and lightweight design to lower lifecycle carbon emissions. Tighnavard et al. [19] demonstrated, based on LCA and Life Cycle Cost (LCC) analysis, that novel engineered wood-steel plate composite structures enhance structural performance while offering significant low-carbon and economic advantages. Xu et al. [20] established a P-GPS-LCA model based on LCA theory to evaluate carbon reduction potential in building components, finding prefabricated buildings had lower emissions than cast-in-situ ones, with emissions decreasing as prefabrication

rates increased; emissions showed a significant linear positive correlation with prefabricated volume and cost. Aiyan et al. [21] developed a carbon emission calculation model for the production and construction stages of prefabricated components using process inventory analysis, with case studies showing lower emissions per unit area for prefabricated concrete composite slabs compared to cast-in-situ slabs, and emissions decreasing with higher prefabrication rates. Xiaocun et al. [22] analyzed a dataset of 403 buildings, assessing the statistics and distribution of Embodied Carbon Intensity (ECI) using a cradle-to-site boundary, revealing that two-thirds of emissions stemmed from structural materials (steel, concrete, prefabricated components); strategies like low-carbon material substitution, material optimization, and cascading use were identified for ECI reduction. Li et al. [23] quantified the carbon emissions of Prefabricated Concrete Buildings (PCBs) using a BIM-based lifecycle accounting system, finding PCBs significantly reduced emissions compared to traditional cast-in-situ buildings, with emissions concentrated in the operation and maintenance phase and negative emissions during demolition and recycling. Li et al. [24] constructed a lifecycle carbon footprint accounting framework for prefabricated buildings based on circular economy principles, verifying through case studies the dominant contribution of material production and transportation stages, and employed data quality indicators and Monte Carlo simulation for uncertainty analysis, identifying key reduction processes like cast-in-place concrete. These studies primarily utilize lifecycle-oriented quantitative methods (LCA, LCC, BIM, process inventory analysis, carbon footprint frameworks) focusing on contributions from novel materials (engineered wood, CFRP composites, recycled concrete), novel structures (precast sandwich panels, semi-sandwich panels, wood-steel composites), or advanced construction methods (prefabrication) to reduce building lifecycle carbon emissions. However, a model explicitly linking structural seismic performance with carbon emissions has yet to be developed. Bridging this gap by establishing a quantitative relationship between seismic performance and carbon emissions is essential for advancing integrated safety-sustainability design methodologies.

The authors' research group has previously conducted systematic experimental investigations on this novel wall system. Quasi-static cyclic tests on individual full-scale WCWs [25] were performed to understand their fundamental hysteretic behavior, including failure mechanisms, bearing capacity, ductility, stiffness degradation, and energy dissipation capacity under various design parameters (concrete layer thickness, steel wire spacing, concrete strength, and axial compression ratio). Subsequently, a shaking table test on a 1:3 scaled three-story WCW building model [26] was carried out to evaluate its overall seismic response under realistic ground motions, capturing dynamic characteristics, acceleration and displacement responses, and damage progression. These prior studies confirmed the favorable mechanical properties and satisfactory seismic performance of WCWs, providing essential experimental data for validating numerical models. However, despite this progress, the absence of standardized seismic performance evaluation criteria and scientifically validated methodologies for quantifying carbon reduction advantages impedes their broader engineering implementation.

This study focuses on WCWs, pursuing two core objectives: establishing standardized criteria for their seismic performance and quantifying their carbon emissions as a function of the design seismic intensity. On this basis, the building structure model is established. After shaking table test and numerical simulation, IDA and quantile regression methods were used to establish a three-layer seismic performance evaluation framework based on inter-story drift ratio and shear force. In addition, a novel four-stage correlation model (seismic intensity-structural response-wall size-carbon emissions) is established to clearly link carbon emissions with seismic intensity indicators and quantify low-carbon benefits under different seismic design schemes. Crucially, carbon

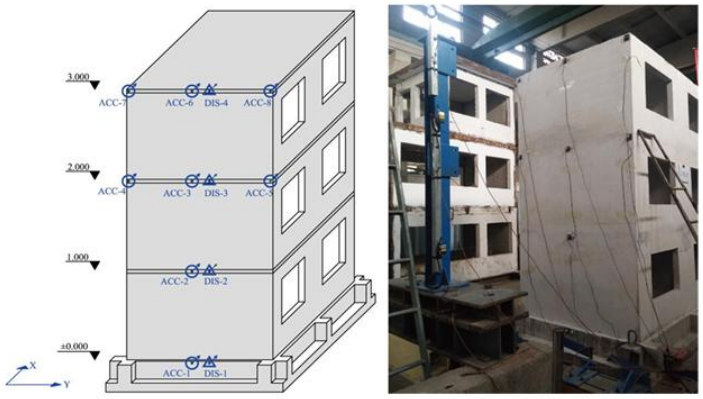

Figure 2. Scaled model shake table test

emissions were directly correlated with seismic intensity measures, revealing the significant impact of seismic hazard levels on low-carbon design outcomes.

2. Seismic performance evaluation of WCW building structures

2.1 Verification of numerical model of WCW building

In the early stage, the research group constructed a 1:3 scale model for shake table testing. The primary load-bearing elements are cast-in-situ WCW panels, integrated with cast-in-situ concrete components (foundations, ring beams, structural columns, floor slabs) to form a semi-prefabricated monolithic system, as shown in Fig. 2 [26]. In this paper, the shaking table test data of WCW building are compared with the numerical model to verify the accuracy of the finite element modeling.

A 3D nonlinear dynamic analysis model of the scaled WCW building structure was developed using the OpenSees platform via the STKO pre/post-processor. Concrete material behavior was modeled using the "Concrete02" constitutive model; steel reinforcement was modeled using "Steel01". The model employed a spatial frame approach: beams, columns, walls, and reinforcement measures were simulated using beam-column elements. Beams and columns used rectangular fiber sections. Square steel tubes reinforcing door/window openings used elastic sections. Shear walls were modeled using membrane fiber elements. Rigid diaphragms ("RigidDiaphragm" constraint) were assigned at each floor level to simulate slab in-plane rigidity. The final model comprised 195 nodes and 390 elements, as shown in Fig. 3. Transient analysis employed the Newmark-β method. Due to rigid diaphragm constraints, the "Transformation" constraint handler and "Newton" algorithm (subspace) were used. Convergence was monitored using tolerance criteria.

Modal analysis was first performed to determine the structure's dynamic characteristics. A comparison of fundamental frequencies between test and simulation is presented in Table 1, showing reasonably small errors and validating the model's basic accuracy.

The maximum acceleration responses at the top floor obtained from STKO FEA under EL-Centro (Basic 7-degree, Rare 8-degree) and Taft (Basic 7-degree, Rare 8-degree) excitations are

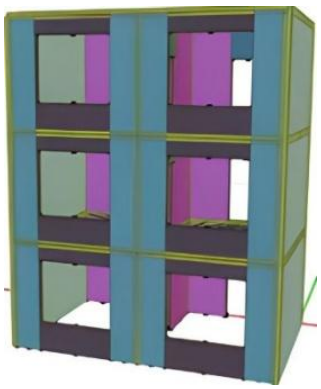

Figure 3. Finite element model of scaled WCW building structure

Table 1. Comparison of fundamental frequencies

Direction	Mode	Test (Hz)	FEA (Hz)	Error (%)
X	1st	10.02	11.20	11.78
	2nd	20.08	21.36	6.37
	3rd	39.07	41.71	6.76

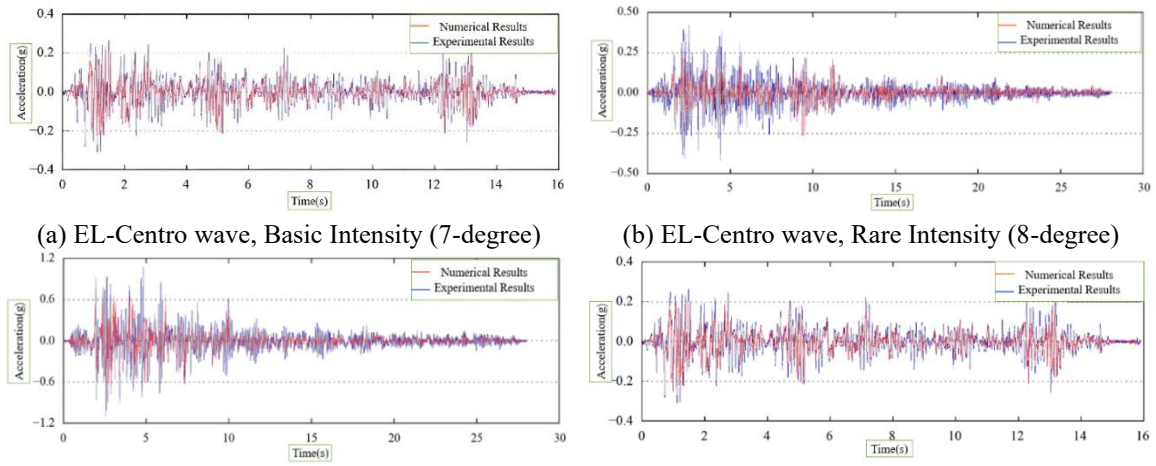

(a) EL-Centro wave, Basic Intensity (7-degree)

(b) EL-Centro wave, Rare Intensity (8-degree)

(c) Taft wave, Basic Intensity (7-degree)

(d) Taft wave, Rare Intensity (8-degree)

Figure 4. Comparison of top floor acceleration time history

compared with shake table test results in Fig. 4. The simulated responses exhibit consistent trends and magnitudes with experimental data, further verifying the reliability of the FE model and material parameter selection. The validation against shake table tests confirms the accuracy of the scaled FE model, providing a reliable basis for subsequent IDA on the full-scale model.

Beyond global response parameters such as natural frequency and acceleration time history, the failure mode observed in the shake table test provides crucial qualitative validation of the numerical model's accuracy. As detailed in the authors' previous work [26], the physical test revealed a clear sequence of damage. Cracks initially appeared at the corners of wall openings on

(a) Cracks around window opening (b) Diagonal cracks on first-floor walls

Figure 5. damage patterns [26]

the first floor at a peak ground acceleration (PGA) of 0.54 g. With increasing intensity up to 0.81 g, extensive diagonal cracks developed predominantly in walls with larger openings (designated W1 and W2 in [26]), forming an "X" pattern characteristic of shear-dominant failure, while upper floors remained largely undamaged. Critically, even at this ultimate stage, the cold-formed thin-walled steel tubes embedded at wall boundaries and around openings effectively arrested crack propagation, preventing through-wall cracking and structural collapse, as illustrated in Fig. 5. This observed failure mechanism—characterized by distributed diagonal cracking without catastrophic disintegration—aligns well with the damage patterns predicted by the numerical model and supports its capability to simulate the inelastic behavior of WCWs.

2.2 Incremental dynamic analysis of WCW building structure

The full-scale prototype building, on which the IDA is based, is a three-story structure with a story height of 3.0 m and a total height of 9.0 m. Its plan dimensions are 4.5 m×7.2 m. The WCWs have a total thickness of 200 mm, consisting of two 50 mm thick concrete wythes and an 80 mm thick expanded polystyrene (EPS) core, reinforced with 2.5 mm diameter galvanized steel wire meshes (50 mm×50 mm grid) and slant connectors. The floor slabs are 120 mm thick. Detailed construction and reinforcement layouts, including the arrangement of thin-walled steel tubes at openings and connections, follow the descriptions in the authors' previous experimental work [26] and are illustrated in Fig. 1 of this manuscript.

A full-scale nonlinear FE model of the WCW building structure was developed in STKO. IDA was performed on this model. Fourteen ground motion records conforming to FEMA P-695 [27] requirements were selected from the provided set. The intensity measure (IM) was the spectral acceleration at the structure's fundamental period with 5% damping, $S_a(T_1,5\%)$. The damage measures (DMs) were the maximum inter-story shear force V and the maximum inter-story drift ratio θ_{max}. The Hunt and Fill algorithm [28] was employed for amplitude scaling. Starting with an initial $S_a(T_1,5\%)$=0.5 g, the scaling increment was set to 0.2 g initially, with a step size increment of 0.05g. When analysis divergence occurred (indicating collapse), interpolation was performed between the largest IM value causing convergence and the smallest IM value causing divergence to pinpoint the collapse point accurately. Further interpolation was applied between converged

Table 2. Example ground motion scaling using Hunt & Fill algorithm

Step No.	Calculation Method	$S_a(T_1,5\%)$ (g)	λ
1	\	0.5	0.773
2	0.5+0.20	0.7	1.082
3	0.7+0.20+0.05×1	0.95	1.468
4	0.95+0.20+0.05×2	1.25	1.932
5	1.25+0.20+0.05×3	1.6	2.473
6	1.6+0.20+0.05×4	2	3.091
7	2+0.20+0.05×5	2.45	3.787
8	2.45+0.20+0.05×6	2.95	Divergent
9	2.45+(2.95-2.45)/3	2.62	Divergent
10	2.45+(2.62-2.45)/3	2.51	3.879
11	(2.45+2)/2	2.225	3.439
12	(2+1.6)/2	1.8	2.782
13	（1.6+1.25)/2	1.425	2.202

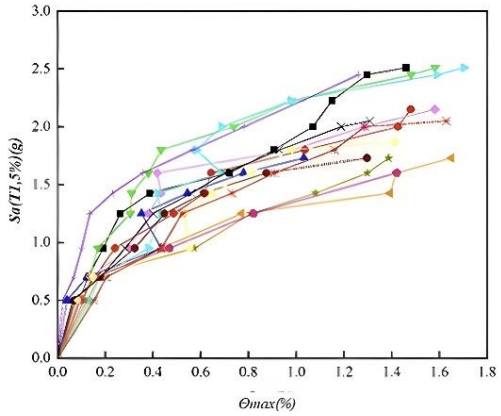

Figure 6. MIR IDA curves

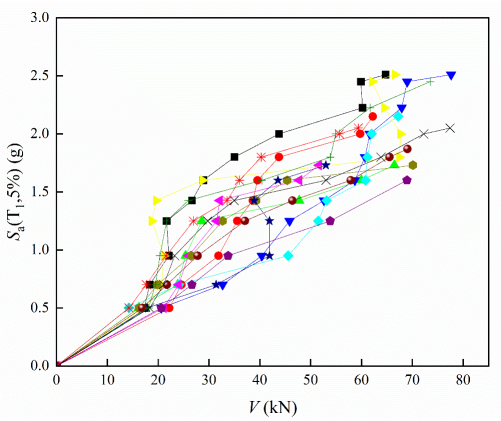

Figure 7. MIF IDA curves

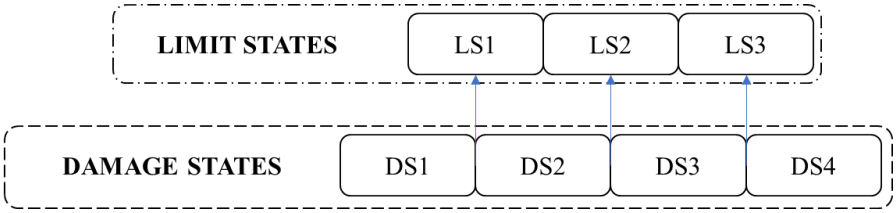

Figure 8. Relationship between damage states and limit states

points at lower IMs to densely populate the IDA curves. The scaling process for one record is exemplified in Table 2.

For each scaled ground motion record, nonlinear time-history analysis was performed. The maximum inter-story drift ratio (MIR) θ_{max} and maximum inter-story shear force (MIF) V were extracted for each IM level. Analysis stopped when divergence occurred (indicating collapse). IDA curves were by plotting DM (θ_{max} or V) versus IM $S_a(T_1,5\%)$ for all 14 records, as shown in Figs. 6 and 7.

Figs. 6 and 7 show that at low IM levels, IDA curves are nearly linear with low dispersion, indicating elastic structural behavior. As $S_a(T_1,5\%)$ increases, the structure enters the inelastic range, curve dispersion increases significantly, and the rate of DM increase slows down, reflecting the uncertainty inherent in ground motions.

2.3 Seismic performance evaluation indices for WCW structure

The seismic performance of the WCW building structure is categorized into four damage states (DS): DS1 (No Damage), DS2 (Moderate Damage), DS3 (Severe Damage), DS4 (Collapse), corresponding to three limit states (LS): LS1 (Immediate Occupancy-IO), LS2 (Life Safety-LS), LS3 (Collapse Prevention-CP). The relationship between damage states and performance levels is illustrated in Fig. 8.

The MIR (θ_{max}) and MIF (V) were selected as engineering demand parameters (EDPs) because they effectively capture the deformation and force demands on the structure, respectively, which are essential for defining damage states. Using the DM Indicator Method [29], limit state thresholds for three performance levels were defined based on the slope evolution of the Incremental Dynamic Analysis (IDA) curve: LS1 (IO) corresponds to a significant change from the initial elastic slope (Ke); LS2 (LS) is identified by a pronounced negative slope or inflection point; LS3 (CP) is reached when the slope $K \leq 0.2Ke$.

MIR serves as a proxy for ductility and deformation capacity, quantifying damage progression across limit states, from 0.06% at LS1 to 1.12% at LS3. These thresholds correspond to physically observable damage mechanisms from quasi-static cyclic tests on individual WCWs [25]: LS1 matches initial flexural cracking; LS2 aligns with significant stiffness degradation and diagonal shear crack dominance; LS3 corresponds to the ultimate displacement near peak load where strength degradation accelerates toward failure.

MIF captures lateral strength evolution through its peak values on IDA curves. Additionally, the changing slope of the IDA curve—the basis for defining the three limit states—implicitly reflects stiffness degradation. The overall IDA curve path, influenced by V and θ_{max}, also embodies the structure's energy dissipation capacity. Thus, establishing probabilistic limits for both EDPs enables an integrated assessment linking global seismic response to cumulative damage states.

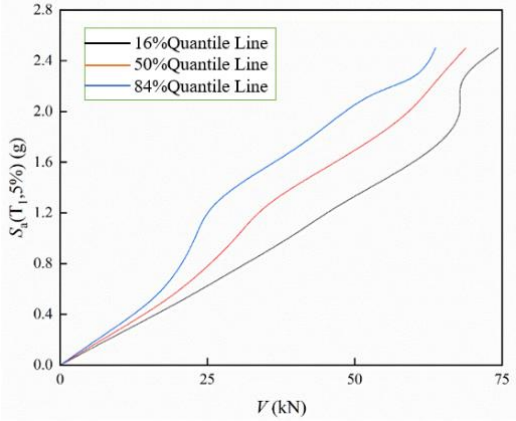

Figure 9. MIF quantile curves

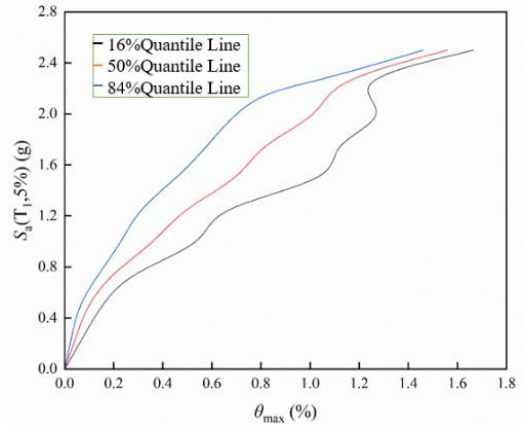

Figure 10. MIR quantile curves

Table 3. Limit state thresholds for performance levels

Limit state parameter	LS1 (IO)	LS2 (LS)	LS3 (CP)
V_{max} (kN)	17.94	29.94	68.79
θ_{max} (%)	0.06	0.70	1.12

To account for record-to-record variability and provide a probabilistic assessment, the IDA data were analyzed using the quantile regression method, specifically conditioning on IM. The conditional probability distribution of DM given IM=x is assumed to be lognormal. Thus, ln (DM|IM=x) follows a normal distribution N(μ,σ), where μ=ln$\eta_{DM|IM}$ and σ=$\beta_{DM|IM}$, (μ is the median, σ is the logarithmic standard deviation of DM given IM=x). Quantile curves corresponding to 16%, 50% (median), and 84% probabilities of exceedance were calculated using Eqs. (1)-(3) and plotted in Figs. 9 and 10 for V_{max} and θ_{max} respectively. The limit state thresholds were determined by applying the DM Indicator Method criteria to the median (50%) quantile curves, resulting in the values listed in Table 3.

$$P\left[DM \le \eta_{DM|IM} | IM = x\right] = p\left[ln\, D\, M \le ln\, \eta_{DM|IM} \,| IM = x\right] = P\left[\left(ln\eta_{DM|IM} - ln\, \eta_{DM|IM}\right)/\beta_{DM|IM} | IM = x\right] = \Phi(0) = 0.5 \tag{1}$$

$$P\left[DM \le \eta_{DM|IM} \cdot e^{+\beta_{DM|IM}} | IM = x\right] = P\left[\left(ln\, \eta_{DM|IM} \cdot e^{+\beta_{DM|IM}} - ln\, \eta_{DM|IM}\right)/\beta_{DM|IM} | IM = x\right] = \Phi(1) = 0.84 \tag{2}$$

$$P\left[DM \le \eta_{DM|IM} \cdot e^{-\beta_{DM|IM}} | IM = x\right] = P\left[\left(ln\, \eta_{DM|IM} \cdot e^{-\beta_{DM|IM}} - ln\, \eta_{DM|IM}\right)/\beta_{DM|IM} | IM = x\right] = \Phi(-1) = 0.16 \tag{3}$$

Table 3 summarizes the limit state thresholds for three performance levels—Immediate Occupancy (IO), Life Safety (LS), and Collapse Prevention (CP)—defined by the MIR (θ_{max}) and MIF (V_{max}). Derived from IDA curves using slope-change criteria, these thresholds (θ_{max}=0.06%, 0.70%, 1.12%; V_{max}=17.94 kN, 29.94 kN, 68.79 kN) correspond to initial flexural cracking, significant stiffness degradation with diagonal shear cracking, and near-collapse conditions, respectively, consistent with quasi-static test observations [25]. Serving as key inputs to the four-stage correlation model in Section 3.2, these performance limits—particularly the CP-level shear force—bridge seismic demands with wall dimensions and carbon emissions, enabling integrated safety-sustainability design optimization.

3. Carbon emission assessment methodology for WCWs

3.1 Structural seismic fragility analysis

The relationship between the intensity measure (IM) and the median engineering demand parameter (EDP), denoted DM, is typically modeled by a power law [30].

$$DM = \alpha(IM)^{\beta} \tag{4}$$

$$\widehat{D} = \alpha(IM)^{\beta} \tag{5}$$

Taking the natural logarithm of both sides yields a linear relationship:

$$ln\, \widehat{D} = a + b\, ln(\, IM) \tag{6}$$

Assuming DM follows a lognormal distribution, its logarithmic mean (η_d) and logarithmic standard deviation (β_d) can be expressed as:

$$\eta_d = In\widehat{D} \tag{7}$$

$$\beta_d = \sqrt{1/(N-2)\sum_{i-1}^{N}(InD - In\widehat{D})} \tag{8}$$

Similarly, the structural capacity C (limit state threshold for an EDP) is also assumed lognormally distributed with median $\hat{C}$ and logarithmic standard deviation β_c:

$$\eta_c = In\hat{C}, \tag{9}$$

$$\beta_c = \sqrt{1/(N-2)\sum_{i-1}^{N}(InC - In\hat{C})}. \tag{10}$$

The conditional probability of failure (exceeding a limit state) given IM is the fragility function P_f:

$$P_f = P(C/D < 1). \tag{11}$$

Defining Z=C-D, failure occurs when Z<0. Z also obeys normal distribution, logarithmic average $\eta z=\eta c-\eta d$, standard deviation $\beta z=\sqrt{\beta c^2+\beta d^2}$, The fragility function is then given by the cumulative distribution function (CDF) of the standard normal distribution:

$$P_f = P(Z<0) = \int_{-\infty}^{0}(1/\beta_Z\sqrt{2\pi})\,exp\,|-0.5[(Z-\eta_Z)/\beta_Z]^2|dZ, \tag{12}$$

$$P_f = \int(1/\sqrt{2\pi})\,exp(-t^2/2)dt = \Phi(-\eta_Z/\beta_Z) = \Phi\left(In\left[\alpha(IM)^{\beta}/\hat{C}\right]/\sqrt{{\beta_c}^2+{\beta_d}^2}\right). \tag{13}$$

Eq. (13) is the calculation formula of the exceedance probability P_f, which can predict the possibility of structural failure within a certain range.

In order to establish the relationship between the seismic intensity index IM and the structural damage index DM, the natural logarithm of $S_a(T_1,5\%)$ is taken as the independent variable, and the natural logarithm of the maximum inter-story shear force is taken as the dependent variable. Based on the dynamic time history analysis results of 14 seismic waves after amplitude modulation, the scatter plot is drawn and the regression analysis is carried out. The analysis curve is shown in Fig.11. The relationship between the maximum inter-story shear force and the seismic intensity index $S_a(T_1,5\%)$ is obtained by regression analysis, as shown in Eqs. (14) and (15).

$$ln(V) = 3.4167 + 0.8711\,ln\left(S_a(T_1,5\%)\right) \tag{14}$$

$$V = 30.469 \times \left(S_a(T_1,5\%)\right)^{0.871} \tag{15}$$

Bring Eq. (15) into Eq. (13), and get the transcendental probability expression:

$$P_f = \Phi\left(\left[30.469 \times \left(S_a(T_1,5\%)\right)^{0.871} - ln\,C\right]/\sqrt{{\beta_c}^2+{\beta_d}^2}\right). \tag{16}$$

Among them, is the logarithmic standard deviation of the capacity parameter C, and is the logarithmic standard deviation of the seismic response parameter D. Referring to the specification HAZUS [31], when IM is $S_a(T_1,5\%)$, the denominator value can be taken as 0.4. According to the maximum inter-story shear force limit, the value of the capacity parameter C is determined, the standard score is calculated, and then the probability of its occurrence is found through the standard normal distribution table, and the exceedance probability corresponding to different performance levels of the structure can be obtained. The (IM, P_f) is plotted in the coordinate system and connected by spline curves. The seismic vulnerability curve of the structure is shown in Fig. 12.

From the shape and position of the fragility curves, it can be observed that the probabilities of exceeding the LS2 (Life Safety) and LS3 (Collapse Prevention) limit states remain relatively low, even at higher intensity levels. This indicates that the WCW building structure possesses a high

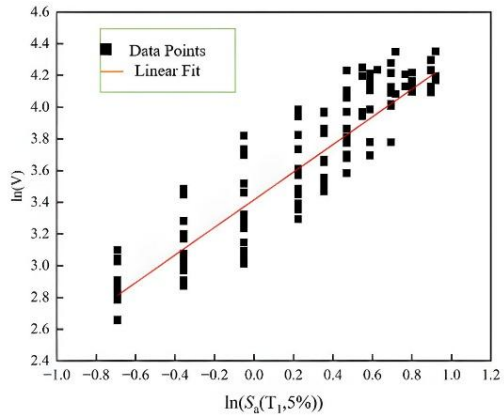

Figure 11. Relationship between $S_a(T_1,5\%)$ and V

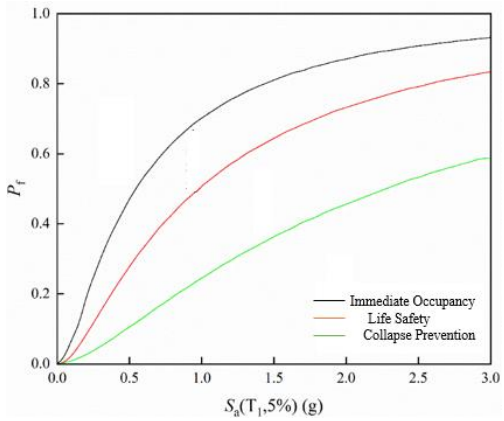

Figure 12. Seismic fragility curves based on V_{max}

margin of safety against severe damage and collapse under strong earthquake excitations. The structure exhibits a gradual damage progression, with a clear separation between limit states, which is desirable for performance-based design. These observations quantitatively demonstrate that the proposed wire-mesh concrete sandwich wall system exhibits favorable seismic resistance and satisfies the requirements for ductile failure mechanisms under moderate to high seismic intensities.

3.2 Theoretical derivation linking seismic intensity and carbon emissions

This section establishes a direct link between seismic performance and carbon emissions, enabling rapid assessment of WCW carbon emissions under different seismic design requirements. The core concept involves four interconnected relationships:

(1) The first relationship between the maximum inter-story shear force and the ground motion intensity index has been introduced in detail in Section 2.1 and rigorous theoretical derivation and analysis have been carried out. The results are shown in Eq. (15).

(2) The second relationship between the maximum inter-story shear force and the wall size is

established. Our research group's previous quasi-static test results show [25] that the bearing capacity is mainly related to the thickness of the concrete layer, the axial compression ratio and the strength of the concrete. Based on the shear bearing capacity formula of inclined section of eccentric compression reinforced concrete shear wall in relevant specifications [32, 33], a modified shear bearing capacity formula of inclined section of eccentric compression reinforced concrete shear wall (Eq. (17)) is proposed:

$$V_m = \left(0.25 f_t b_{eff} h_{eff} + 0.13 N b_{eff} l f_c\right)/(\alpha - 0.5) + 0.1 f_{tu} \frac{A_s}{S_r} h_{eff}. \tag{17}$$

Among them, V_m is the shear bearing capacity of the steel wire mesh concrete house structure, respectively, b_{eff} and h_{eff} are the wall section width and effective height, f_t is the concrete tensile strength design value, f_{tu} is the steel wire tensile strength design value, S_r and A_s are the wall in the same horizontal section of the steel wire section area and spacing, α is the shear span ratio of the section, α<1.5, is given 1.5 α>2.2, is given 2.2. N is the wall axial compression ratio, l is the wall length, f_c is the concrete compressive strength design value.

Let the maximum shear design value of the sandwich wall be equal to the shear bearing capacity, then $V=V_m/\gamma_{RE}$, γ_{RE} is the seismic adjustment coefficient of the bearing capacity, which improves the economy under the premise of ensuring "no collapse under major earthquakes", and guides the structure to form an ideal energy dissipation mechanism. Therefore, the second relationship formula is:

$$V = V_m/\gamma_{RE} = \left(\left(0.25 f_t b_{eff} h_{eff} + 0.13 N b_{eff} l f_c\right)/(\alpha - 0.5) + 0.1 f_{tu} \frac{A_s}{S_r} h_{eff}\right)/\gamma_{RE}. \tag{18}$$

(3) The model establishes the third relationship – linking ground motion intensity indices to wall size-by integrating the first relationship (seismic intensity and shear force) and second relationship (shear force and wall size) through the maximum inter-story shear force. Therefore, the third relationship formulas are:

$$\left(\left(0.25 f f_t b_{eff} h_{eff} + 0.13 N b_{eff} l f_c\right)/(\alpha - 0.5) + 0.1 f_{tu} \frac{A_s}{S_r} h_{eff}\right)/\gamma_{RE} = 30.469 \times \left(S_a(T_1, 5\%)\right)^{0.871}, \tag{19}$$

$$b_{eff} = \gamma_{RE}(\alpha - 0.5) \frac{f(IM) - A}{B}, \tag{20}$$

Among them, A=$0.1 f tu \frac{As}{Sr} heff$, B=$0.25 f theff$+$0.13 N lfc$, $f(IM)$=30.469×$S_a(T_1,5\%)^{0.871}$.

(4) The study establishes the fourth relationship between wall size and carbon emissions. Through the third relationship, the calculation formula of wall size and ground motion intensity index can be used to calculate the volume of structural concrete, and the carbon emissions of concrete per unit volume can be known. Therefore, the relationship between wall size and carbon emissions can be deduced, and the relationship between ground motion intensity index and carbon emissions can be directly derived. So we can get:

$$[C_1] = \delta_1\left[V\left(b_{eff}\right)\right] = \delta_1\left[l \times h_{eff} \times \gamma_{RE}(\alpha - 0.5) \frac{f(IM) - A}{B}\right], \tag{21}$$

$$[C] = [C_1] + \sum_{i=2}^{n} [C_i]. \tag{22}$$

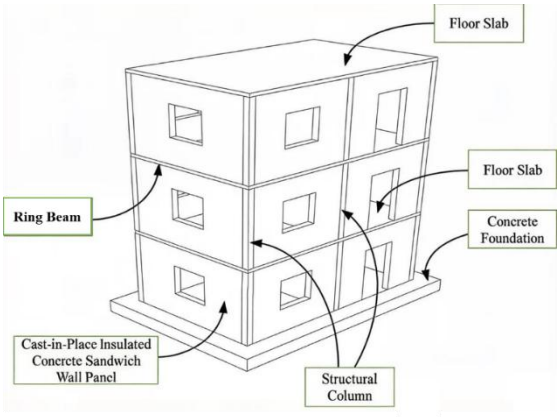

Figure 13. Wire-mesh concrete sandwich wall building structure

Table 4. Material carbon emission factors

Material	Emission factor (EF)	Unit
C30 concrete	295	kg CO_2e/m^3
Expanded polystyrene (EPS)	5020	kg CO_2e/t
Steel wire	2.46	kg CO_2e/kg

Among them, δ_1 is the carbon emission of concrete per unit volume, $V(b_{eff})$ is the calculation formula of concrete volume with plate thickness as variable, and C_i is the carbon emission value of other materials.

3.3 Engineering case study: Carbon emission assessment

A 3-story, single-bay, double-bay WCW building (total height 9 m, story height 3m) is considered. Key element dimensions: ring beams 200×200 mm, structural columns 200×200 mm, WCW thickness 200 mm, floor slab 120 mm. The layout is shown in Fig. 13.

The carbon emission of the sandwich wall is equal to the sum of the carbon emission of concrete, the carbon emission of polystyrene foam board and the carbon emission of low carbon galvanized steel wire. The carbon emission factor of the wall contains the material [34] as shown in Table 4.

Among them, the carbon emission of concrete is equal to the volume of concrete multiplied by the carbon emission per unit volume of concrete. The carbon emission of polystyrene foam board is equal to the product of the volume of polystyrene foam board, the density of polystyrene foam board and the carbon emission per unit volume of polystyrene foam board. The carbon emission of low carbon galvanized steel wire is equal to the product of the total length of low carbon galvanized steel wire, the density of low carbon galvanized steel wire and the carbon emission per unit volume of low carbon galvanized steel wire.

For example, under the condition of 7 degree fortification, taking the wall with a size of 3 m×4.5 m×0.2 m as an example, the shear span ratio λ is 1.5, the compressive strength of concrete f_c is 30 Mpa, the axial compression ratio N is 0.06, the strength of steel wire f_{tu} is 549 Mpa, the tensile strength of concrete f_t is 5 Mpa, the cross-sectional area of steel wire A_s is 4.908 mm^2,

h_{eff}=3000 mm, $S_a(T_1,5\%)$ is 3.818 g, the span l is 4500 mm, and the spacing of steel wire S_r is 150 mm, b_{eff}=59.9 mm.According to the determined seismic strength index, combined with the first relationship model, the second relationship model, the third relationship model and the fourth relationship model, the volume of concrete in the sandwich wall, the volume of polystyrene foam board and the total length of low carbon galvanized steel wire are determined.

The volume of concrete is 1.62 m^3; the density of polystyrene foam board is 34 kg/m^3 (0.034 t/m), and the volume is 1.08 m^3. The density of 2.5mm low carbon galvanized steel wire is 3.85 kg/100m (0.0385 kg/m), and the total length of steel wire is 458 m. From the Eq. (21), (22), the carbon emission of the steel wire mesh concrete building structure is calculated as follows:

$$C = 1.62m^3 \times 295\ kgCO_2e/m^3 + 1.08\ m^3 \times 0.034\ t/m^3 \times 5020\ kgCO_2e/t + 458\ m \times 0.0385\ kg/m \times 2.46\ kgCO_2e/kg \approx 705.6\ kg. \quad (23)$$

The carbon emission value of the reinforced concrete shear wall of the same size is approximately 1199.88 kg. This indicates that the steel wire mesh concrete sandwich wall achieves a 41.19% reduction in carbon emissions compared to the reinforced concrete shear wall. Based on this finding, it can be further inferred that the overall structural system of steel wire mesh concrete buildings offers significant carbon reduction potential relative to conventional reinforced concrete structures. Therefore, WCWs demonstrate strong potential for widespread application as a green building solution across various construction types.

4. Conclusions

This study systematically investigated the seismic performance evaluation criteria and carbon emission assessment methodology for wire-mesh concrete sandwich walls (WCWs) through experimental testing, numerical simulation, and theoretical derivation. The main conclusions are:

(1) Through incremental dynamic analysis of a WCW building structure validated by shake table tests [21], the response characteristics under earthquake excitation were revealed. Based on the quantile curve method, the discreteness of the maximum inter-story shear force (V) and drift ratio (θ_{max}) was quantified. Three performance level limits—Immediate Occupancy (IO), Life Safety (LS), and Collapse Prevention (CP)—were established based on IDA curve slope changes, yielding θ_{max}=0.06%, 0.70%, 1.12% and V=17.94 kN, 29.94 kN, 68.79 kN, respectively. The structure exhibits a flexural-shear composite failure mode under strong earthquakes, with slant steel wires effectively transmitting shear forces and delaying concrete wythe separation, consistent with observations from quasi-static tests [25]. The overall seismic performance meets code requirements.

(2) A novel four-stage correlation model (seismic intensity-structural response-wall dimensions-carbon emissions) was developed, establishing a direct quantitative link between seismic performance demands and carbon emissions. A case study demonstrated that WCWs reduced embodied carbon emissions by 41.19% compared to traditional RC shear walls. This low-carbon advantage primarily arises from the lightweight design (EPS insulation core, efficient wire mesh reinforcement) and reduced concrete volume. However, higher seismic intensity demands increase material requirements and consequently carbon emissions, highlighting the need for integrated safety-sustainability optimization.

The outcomes of this research provide a theoretical foundation for the engineering application of WCWs, fostering the integrated advancement of structural safety and low-carbon performance

in green building design. Future work should incorporate comprehensive life cycle assessment and extend the methodology to other sandwich wall configurations.

Acknowledgment

This research was funded by Hebei Provincial Higher Education Scientific Research Project (CXZX2025050); Natural Science Foundation of Hebei Province for Distinguished Young Scholars (E2022210084); the S&T Program of Hebei (CN) (216Z5402G); Natural Science Foundation of Hebei Province (E2022210095; E2024210049); the Earthquake Science and Technology Program of Hebei Province (grant no. DZ2025092800001).

References

1. Hu, Z.W., Xu, Z.D., Zhang, L.Y., He, J.X., Chen, Z.H., Miao, Q.S., Li, W.F. (2025). Full-scale shaking table test on a precast sandwich wall panel structure with a high-damping viscoelastic isolation and mitigation device. Engineering Structures, 329, 119797-119797. https://doi.org/10.1016/j.engstruct.2025.119797.
2. He, J.X., Xu, Z.D., Hu, Z.W., Zhang, L.Y., Li, Q.Q., Dong, Y.R., Milani, G. (2025). A novel multi-dimensional viscoelastic mitigation device: Shake table tests and numerical assessment of precast concrete sandwich wall panel structure. Engineering Structures, 336, 120388-120388. https://doi.org/10.1016/j.engstruct.2025.120388.
3. Yan, W., Zhang, Y., Lou, G., Sun, K. (2025). Seismic behavior and design method of a novel UHPC panel sandwich shear wall: Experimental and numerical study. Engineering Structures, 334, 120243. https://doi.org/10.1016/j.engstruct.2025.120243.
4. Li, M., Li, Z., Gao, C., Ma, H. (2025). Experimental and numerical study on the seismic performance of prefabricated ceramsite foam concrete sandwich shear wall. Structures, 75, 108838. https://doi.org/10.1016/j.istruc.2025.108838.
5. Sisti, R., Corradi, M., Balsamo, A., Di Ludovico, M., Prota, A., Speranzini, E., Molinari, A. (2023). Analysis of the seismic vulnerability and innovative retrofit solutions of cavity brickwork walls. Construction and Building Materials, 409, 134018. https://doi.org/10.1016/j.conbuildmat.2023.134018.
6. Chougule, S.S., Bharti, S.D., Shrimali, M.K., Datta, T.K. (2024). Seismic behavior of precast wall slab wall structure under near and far field earthquakes. Bulletin of Earthquake Engineering, 22(14), 6991-7013. https://doi.org/10.1007/s10518-024-02030-8.
7. Xu, G., Guo, T., Li, A. (2023). Seismic performance and fragility analysis of precast concrete sandwich wall structure. Journal of Earthquake Engineering, 27(2), 410-433. https://doi.org/10.1080/13632469.2021.2003272.
8. Zhang, X., Ren, G., Zhang, E. (2023). Experimental study on seismic performance of thin-walled steel-straw board composite walls with built-in steel plate. Journal of Building Engineering, 76, 107407. https://doi.org/10.1016/j.jobe.2023.107407.
9. Yin, F., Cao, W.L., Wang, R.W., Weng, H.F., Liu, Y.B. (2022). Seismic behavior of prefabricated concrete filled steel tube-bordered monolayer reinforced shear wall. Journal of Constructional Steel Research, 194, 107328. https://doi.org/10.1016/j.jcsr.2022.107328.
10. Herrera, J.P., Bedoya-Ruiz, D., Hurtado, J.E. (2020). Performance-based seismic assessment of precast ferrocement walls for one and two-storey housing. Engineering Structures, 214, 110589. https://doi.org/10.1016/j.engstruct.2020.110589.
11. Guo, W., Zhai, Z., Cui, Y., Yu, Z., Wu, X. (2019). Seismic performance assessment of low-rise precast wall panel structure with bolt connections. Engineering Structures, 181, 562-578.

https://doi.org/10.1016/j.engstruct.2018.12.060.
12. Vasishta, T., Mehany, M.H., Killingsworth, J. (2023). Comparative life cycle assesment (LCA) and life cycle cost analysis (LCCA) of precast and cast-in-place buildings in United States. Journal of Building Engineering, 67, 105921. https://doi.org/10.1016/j.jobe.2023.105921.
13. Xu, M., Chang, Y. (2025). Benchmarking the embodied carbon dioxide footprint of prefabricated buildings in China: A high-resolution structural and spatial quantification. Energy and Buildings, 351, 116771. https://doi.org/10.1016/j.enbuild.2025.116771.
14. Dong, Y., Man, Q., Zhang, Y., Chang, Y. (2025). Optimisation route of embodied carbon emissions and cost of prefabricated buildings: A case study of prefabricated shear wall residential structures. Energy and Buildings, 343, 115919. https://doi.org/10.1016/j.enbuild.2025.115919.
15. Gaibor, N., Mateus, R., Leitao, D., Cristelo, N., Miranda, T., Pereira, E.N., Cunha, V.M. (2023). Sustainability assessment of half-sandwich panels based on alkali-activated ceramic/slag wastes cement versus conventional building solutions. Journal of Cleaner Production, 389, 136108. https://doi.org/10.1016/j.jclepro.2023.136108.
16. Ding, Y., Pang, Z., Lan, K., Yao, Y., Panzarasa, G., Xu, L., ..., Hu, L. (2022). Emerging engineered wood for building applications. Chemical Reviews, 123(5), 1843-1888. https://doi.org/10.1021/acs.chemrev.2c00450.
17. Hao, J.L., Cheng, B., Lu, W., Xu, J., Wang, J., Bu, W., Guo, Z. (2020). Carbon emission reduction in prefabrication construction during materialization stage: A BIM-based life-cycle assessment approach. Science of the Total Environment, 723, 137870. https://doi.org/10.1016/j.scitotenv.2020.137870.
18. Sojobi, A.O., Liew, K.M. (2022). Multi-objective optimization of high performance bio-inspired prefabricated composites for sustainable and resilient construction. Composite Structures, 279, 114732. https://doi.org/10.1016/j.compstruct.2021.114732.
19. Balasbaneh, A.T., Sher, W., Yeoh, D. (2022). Recommending a new building structure to alleviate environmental impact in tropical climates: increasing the use of wood in construction. The International Journal of Life Cycle Assessment, 27(7), 885-901. https://doi.org/10.1007/s11367-022-02074-5.
20. Xu, A., Zhu, Y., Wang, Z. (2024). Carbon emission evaluation of eight different prefabricated components during the materialization stage. Journal of Building Engineering, 89, 109262. https://doi.org/10.1016/j.jobe.2024.109262.
21. Xu, A., Zhu, Y., Wang, Z., Zhao, Y. (2023). Carbon emission calculation of prefabricated concrete composite slabs during the production and construction stages. Journal of Building Engineering, 80, 107936. https://doi.org/10.1016/j.jobe.2023.107936.
22. Zhang, X., Li, Y., Chen, H., Yan, X., Liu, K. (2023). Characteristics of embodied carbon emissions for high-rise building construction: A statistical study on 403 residential buildings in China. Resources, Conservation and Recycling, 198, 107200. https://doi.org/10.1016/j.resconrec.2023.107200.
23. Li, X.J., Xie, W.J., Xu, L., Li, L.L., Jim, C.Y., Wei, T.B. (2022). Holistic life-cycle accounting of carbon emissions of prefabricated buildings using LCA and BIM. Energy and Buildings, 266, 112136. https://doi.org/10.1016/j.enbuild.2022.112136.
24. Li, C.Z., Tam, V.W., Lai, X., Zhou, Y., Guo, S. (2024). Carbon footprint accounting of prefabricated buildings: A circular economy perspective. Building and Environment, 258, 111602. https://doi.org/10.1016/j.buildenv.2024.111602.
25. Qiao, W., Yin, X., Zhao, S., Wang, D. (2019). Cyclic loading test study on a new cast-in-situ insulated sandwich concrete wall. PloS one, 14(11), e0225055. https://doi.org/10.1371/journal.pone.0225055.
26. Qiao, W., Kang, J., Wang, D., Yuan, J., Wang, Z. (2021). Shaking table test on insulated sandwich concrete wall building structure. Journal of Building Engineering, 37, 102165. https://doi.org/10.1016/j.jobe.2021.102165.
27. Applied Technology Council (2009). Quantification of building seismic performance factors. US Department of Homeland Security, Federal Highway Administration (FHWA) Office of Infrastructure Research and Development, Washington, D.C., USA.
28. Vamvatsikos, D., Cornell, C.A. (2004). Applied incremental dynamic analysis. Earthquake Spectra, 20(2), 523-553. https://doi.org/10.1193/1.1737737.

29. Vamvatsikos, D., Cornell, C.A. (2002). Incremental dynamic analysis. Earthquake Engineering & Structural Dynamics, 31(3), 491-514. https://doi.org/10.1002/eqe.141.
30. Gong, S.L. (2010). Handbook of seismic design for buildings (2nd edition). China Architecture & Building Press, Beijing, China.
31. Federal Highway Administration (FHWA) (2003). Multi-hazard loss estimation methodology, earthquake model. Federal Highway Administration (FHWA) Office of Infrastructure Research and Development, Washington, D.C., USA.
32. Ministry of Housing and Urban-Rural Development of the People's Republic of China (2010). GB 50010-2010: Code for design of concrete structures. China Architecture & Building Press, Beijing, China.
33. Ministry of Housing and Urban-Rural Development of the People's Republic of China (2010). JGJ 3-2010: Technical specification for concrete structures of tall buildings. China Architecture & Building Press, Beijing, China.
34. Zhao, Y., Liu, L., Yu, M. (2023). Comparison and analysis of carbon emissions of traditional, prefabricated, and green material buildings in materialization stage. Journal of Cleaner Production, 406, 137152. https://doi.org/10.1016/j.jclepro.2023.137152.